frontiers in Materials

ORIGINAL RESEARCH
published: 21 January 2022
doi: 10.3389/fmats.2021.775027

Synthesis of Fibrous Micro-nano Hierarchical Porous Cerium Dioxide Materials by the Impregnation and Thermal Decomposition Method and Its Enhanced Photocatalytic Activity

Meng Zhang[1], *Xingwang Chen*[1], *Min Zu*[1], *Yuanzheng Tang*[1], *Chengbao Liu*[1], *Wanfei Li*[2]* *and Feng Chen*[1]*

[1]*Jiangsu Key Laboratory for Environment Functional Materials, School of Materials Science and Engineering, Suzhou University of Science and Technology, Suzhou, China,* [2]*Suzhou Key Laboratory for Nanophotonic and Nanoelectronic Materials and Its Devices, Suzhou University of Science and Technology, Suzhou, China*

OPEN ACCESS

Edited by:
Tao Xian,
Qinghai Normal University, China

Reviewed by:
Zuming He,
Changzhou University, China
Yuxiang Yan,
Nanjing University, China

***Correspondence:**
Wanfei Li
wfli2018@mail.usts.edu.cn
Feng Chen
ujschenfeng@163.com

Specialty section:
This article was submitted to Semiconducting Materials and Devices, a section of the journal Frontiers in Materials

Received: *13 September 2021*
Accepted: *29 October 2021*
Published: *21 January 2022*

Citation:
Zhang M, Chen X, Zu M, Tang Y, Liu C, Li W and Chen F (2022) Synthesis of Fibrous Micro-nano Hierarchical Porous Cerium Dioxide Materials by the Impregnation and Thermal Decomposition Method and Its Enhanced Photocatalytic Activity. Front. Mater. 8:775027. doi: 10.3389/fmats.2021.775027

Fibrous micro-nano hierarchical porous cerium dioxide materials were prepared from oriental paperbush flower stems by impregnation and thermal decomposition methods. Thermogravimetric analyzer (TG, DSC), field emission scanning electron microscopy (FESEM), X-ray diffraction (XRD), transmission electron microscopy (TEM), N_2 adsorption-desorption isothermals, temperature-programmed reduction (TPR), and UV-Vis spectrophotometer were used to characterize the thermal decomposition behavior, microstructure and photocatalytic properties of fibrous micro-nano hierarchical porous cerium dioxide materials. The results proved that the achieved products retained a fibrous morphology similar to oriental paperbush flower stems with the original biotemplate in material completely removed. The average diameter of CeO_2 particles on the surface of the material is about 9 nm, and the large specific surface area is around 55.6 m^2/g. UV-Vis absorption spectra showed that the fibrous micro-nano hierarchical porous cerium dioxide materials have high light absorption capacity and can respond to simulated sunlight. The effects of initial dye concentration, catalyst concentration, pH value, cycle number, and irradiation time on the photocatalytic activity of fibrous micro-nano hierarchical porous cerium dioxide materials for the photo-degradation of methylene blue under simulated solar irradiation were systematically studied. A reasonable photocatalytic mechanism is proposed based on the experimental results and theoretical analysis. This strategy can be extended to synthesize other broad bandgap semiconductor oxides with high photocatalytic activity for the photo-degradation of organic dyes under simulated solar irradiation.

Keywords: fibrous, cerium dioxide, photocatalytic activity, photocatalytic mechanism, organic dye

INTRODUCTION

With the development of society and the progress of industry, the pollution caused by varied organic dyes is becoming worse, which results in more attention being paid to environmental and energy issues (Chen et al., 2020; Ge et al., 2021). Scientists are committed to enhancing the living environment of mankind and creating better living conditions, and it is imperative to solve the environmental problems caused by industrial development (Chenab et al., 2020; Pooja and Chowdhury, 2021). Recently, pollution, especially organic dyes afecting water resources, has become quite serious. With the background of energy utilization and environmental protection, the photo-degradation of organic pollutants has been actively studied (Medda et al., 2020; Cheng et al., 2021a; Wang et al., 2021a). To reduce the pressure on the environment caused by organic pollutants, many processes including ozone-oxidation method, photo-degradation method, activated-carbon adsorption method, and so on have been designed to degrade the organic pollutants (Caballero-Espitia et al., 2020; Wang et al., 2021b; Wang et al., 2021c). Among these methods, the photo-degradation method is an efficient method to degrade organic dyes from wastewater. Therefore, using the photo-degradation method to study the degradation of organic pollutants from wastewater has important research significance.

The core of the photo-degradation method is to select suitable photocatalysts to degrade organic dyes from wastewater (Wang et al., 2020a; Cheng et al., 2021b; Jiménez-Almarza et al., 2021). Cerium dioxide (CeO_2) is a highly efficient photocatalyst, which shows unique advantages in the degradation of various organic dyes (Gao et al., 2018a; Gong et al., 2019; Murali et al., 2019; Li et al., 2021). However, CeO_2 has a large bandgap and can only respond to ultraviolet light, which greatly restricts its application in the field of photocatalysis. (Wang et al., 2021d; Han et al., 2021). Therefore, it is of great significance to develop a new synthesis route to synthesize the CeO_2 photocatalyst with a special defect structure and study its photocatalytic activity. Lately, the biological template method prepared by inorganic functional materials has become a novel technology to produce the inorganic materials used as photocatalysts (Ai et al., 2021; Kulshrestha et al., 2021). Compared with other preparation methods, the biological template method has the advantages of green environmental protection, a simple process, low cost, and easy mass production. The technique is inspired by the development of biological mineralization and it is the method for preparing inorganic materials with controllable structures. The natural existence and special micromorphology of various biological matters are used as a template, with the introduction of inorganic particles by immersion and the removal of the template by calcination, which is aimed to prepare nano-materials with unique bionic morphology. The structure and properties of the inorganic materials synthesized by the biological template method are highly dependent on the structure and properties of the original biological template. The biological materials possess an inherent hierarchical porous structure, large surface area, light weight, high permeability, and any number of other properties. The chemical composition of the organism and the special microstructure can provide a stable environment for the synthesis of CeO_2 photocatalyst. However, no researchers have yet used the natural biological structure as a template to synthesize a CeO_2 photocatalyst and study its photocatalytic activity. Therefore, the selection of a suitable natural biological structure as a template can be prepared for the industrial production of high-performance CeO_2 photocatalyst.

In this paper, oriental paperbush flower stems were utilized to synthesize the CeO_2 materials with a micro-nano hierarchical structure with high photocatalytic activity for the photo-degradation of methylene blue dye under simulated solar irradiation. The phase purity, microstructure, morphology, optical properties, and photocatalytic activity of micro-nano hierarchical porous cerium dioxide materials were systematically studied. The effects of catalyst concentration, dye concentration, pH value, and stability on the photocatalytic activity of micro-nano hierarchical porous cerium dioxide materials were also studied. The results showed that the prepared micro-nano hierarchical porous cerium dioxide materials can preserve and duplicate the microstructure of the original biological template and exhibit excellent photocatalytic activity for the photo-degradation of methylene blue dye under simulated solar irradiation.

EXPERIMENTAL PROCEDURES

Materials Preparation

All the reagents including $Ce(NO_3)_3{\cdot}6H_2O$, hydrochloric acid anhydrous, and ethanol were purchased from Sinopharm Chemical Reagent Co. Ltd. and the oriental paperbush flower stems were picked from the campus. After being washed by deionized water three times or more, the oriental paperbush flower stems were put in a percentage of anhydrous ethanol solution which to was added a certain amount of hydrochloric acid and were left to stand for 24 h, then this step was repeated three times to get experimental available biological templates. Next, the right amount of oriental paperbush flower stems were impregnated into 0.1 mol/L $Ce(NO_3)_3{\cdot}6H_2O$ solution for 72 h and dried at room temperature, the matter obtained in this step was named the precursor for material synthesis. After repeating the above steps three times, the third drying product was heated to 600°C in a muffle furnace for 200 min. After these processes, the micro-nano hierarchical porous cerium dioxide materials were obtained. To make a comparison, with other conditions unchanged, the cerium dioxide standard samples were obtained by heating pure cerium precursor to 550°C for 200 min in the muffle furnace.

Material Characterization

A thermogravimetric analyzer (TG-DSC TG 209 F3, Netzsch) of fibrous micro-nano hierarchical porous cerium dioxide materials was used to measure the weight changes of precursor for material synthesis during the calcination process. The morphology and various other information about the fibrous micro-nano hierarchical porous cerium dioxide materials were characterized by the Hitachi S4800 type field emission scanning electron microscopy (FESEM) and JEM-2100 type

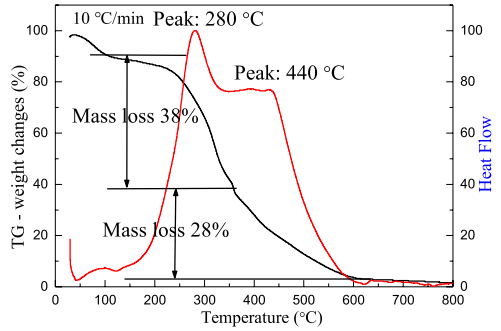

FIGURE 1 | TG-DSC curves of oriental paperbush flower stems/cerium nitrate precursor.

transmission electron microscopy (TEM). The phase structure of fibrous micro-nano hierarchical porous cerium dioxide materials was identified by a Rigaku D/max 2500 PC type X-ray diffraction by using Cu Kα radiation at 40 kV and 40 mA with a scanning rate of 5(°) at 2θ/min which ranges from 20° to 80°. The specific surface area and pore-size distribution of fibrous micro-nano hierarchical porous cerium dioxide materials were calculated by using the BET, ASAP-2010C Brunauer-Emmett-Teller method. A TP-5000 analyzer with a TCD detector (Tianjin, China) was used to determine the temperature-programmed reduction (TPR) of fibrous micro-nano hierarchical porous cerium dioxide materials. The TPR profile of the powder (about 100 mg) was recorded between 20°C and 780°C at a heating rate of 10°C/min.

Photocatalytic Experiments

Methylene blue dye, which is difficult to degrade under natural conditions, was used to detect the photocatalytic activity of fibrous micro-nano hierarchical porous cerium dioxide materials. Before the photo-degradation experiment, adsorption experiments in dark conditions for 30 min were performed to distinguish the change of dye concentration caused by adsorption. A measure of 400 ml of methylene blue solution with a concentration of 10, 50, 100, 150, 200, or 250 mg/L was poured into the photoreactor, and 0.2, 0.4, 0.6, 0.8, 1.0, 1.2, or 1.4 g/L of fibrous micro-nano hierarchical porous cerium dioxide materials was weighed and added into the reactor, and magnetic stirring was carried out simultaneously under the simulated sunlight irradiation with the wavelength of 320–780 nm. Samples were taken at intervals, and the supernatant was removed after centrifugation. The absorbance of methylene blue was measured at 642 nm by the Shimadu Company's UV-Vis spectrophotometer UV-2450. The degradation percentage (D%) of the solution was calculated by the following formula:

$$D\% = \frac{A_0 - A}{A_0} \times 100\% \quad (1)$$

A0 is the absorbance of initial dye concentration, A is the absorbance of the dye after degradation. Simultaneously, different pH values and cyclic stability experiments were performed.

RESULTS AND DISCUSSION

TG-DSC Analysis

Figure 1 shows the TG-DSC curves of oriental paperbush flower stems/cerium nitrate precursor. The black curve in the figure reflects the thermal weight loss of oriental paperbush flower stems/cerium nitrate precursor as the temperature increased, while the red curve represented the changes of the heat flow in the oriental paperbush flower stems/cerium nitrate precursor. From the differential thermal analysis curve in the figure, the weight of the sample system was observed to decrease slightly when the temperature was about 100°C, and there was an insignificant endothermic peak in the heat flow curve, which could be regarded as part of the weight loss caused by the removal of adsorbed water in the complex. (Wang et al., 2013). While two obvious exothermic peaks appeared at 280 and 440°C, and the weight loss of the composite was observed on the corresponding weight loss curves, where the rate of weight loss was 38 and 28%, respectively. The weight loss phenomenon of the composite at 250–350°C can be considered as caused by the carbonization of the organic components in the stem (Zhang et al., 2009a; Zhang et al., 2009b). The observed weight loss between 350 and 600°C was due to the reaction of carbides with oxygen to produce gases such as carbon dioxide (Wu et al., 2004; Xian et al., 2009). The sample was decomposed completely at about 600°C, the quality remained constant. Therefore, the optimum calcination temperature for the selected material is 600°C, at which point the template was completely removed to obtain the pure cerium oxide material.

Microstructure Analysis

Figure 2 presents SEM images of oriental paperbush flower stems and the micro-nano hierarchical ceria material synthesized from oriental paperbush flower stems. In **Figures 2A,B**, the products exhibited irregularly arranged long fibrous structures on the micro-morphology. The length of a single fiber was upward of 100 μm and the fiber radius was about 5–10 μm. In addition, the single fibers intertwined with each other, indicating that the prepared cerium oxide material completely retains the long fibrous structure of the pilose anthers stigma cells completely. Further observation of **Figures 2C,D** showed that the long fibers possessed a lamellar structure, and the edges of these lamellar structures underwent significant warping due to inconsistencies in the material and transverse and longitudinal shrinkage during the subsequent calcination. **Figure 2D** shows the magnified image of the area of the micro-nano hierarchical ceria materials. From the rupture of the fibrous structure in the figure, it can be seen that the inside of the material was hollow structure, which was caused by the curling of the single fiber. The outer surfaces of the fibrous structure were in the shape of burr structures. The presence of the burr structures indicated that in the cerium nitrate precursor after the impregnation–calcination progress the microstructure of the original template was perfectly reproduced. Moreover, these massive skin needles can significantly increase the BET specific surface area of the material and provide more catalytic active sites to promote adsorption of dye, thereby increasing the catalytic activity of the micro-nano hierarchical ceria materials.

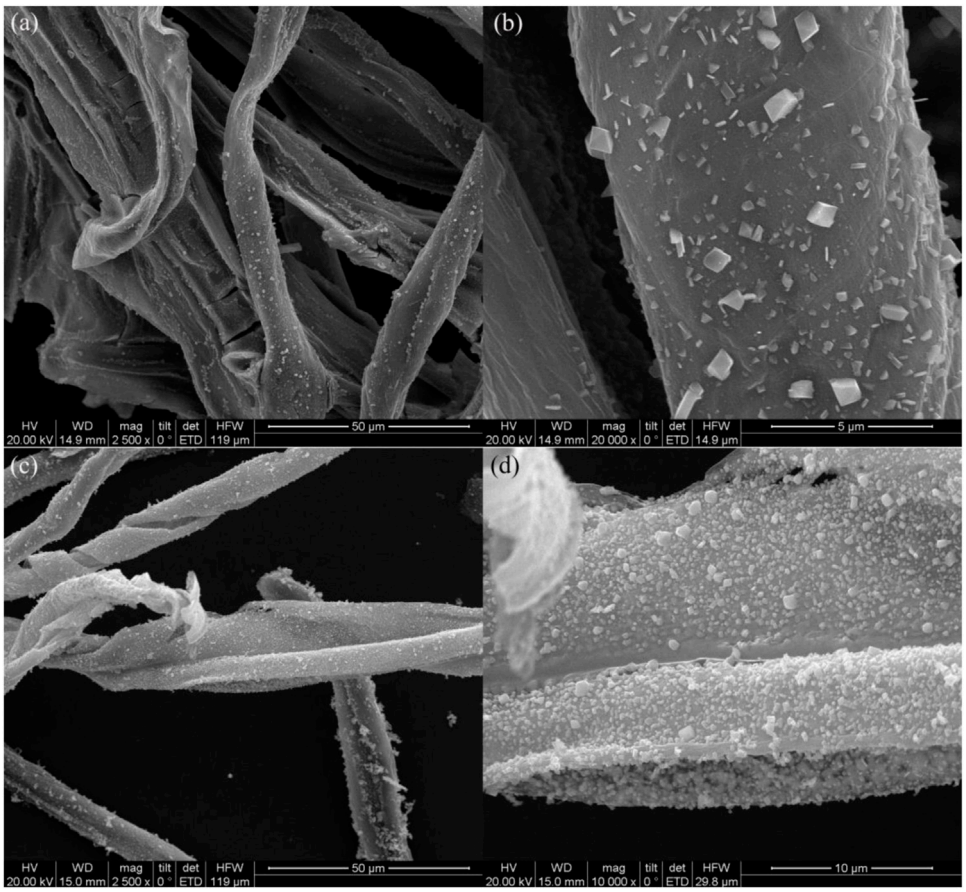

FIGURE 2 | SEM images of the biomimetic structure of oriental paperbush flower stems **(A, B)**, and the micro-nano hierarchical ceria materials **(C, D)**.

The composition of micro-nano hierarchical ceria materials can be observed from **Figures 3A,B**. The surface of micro-nano hierarchical ceria materials was like the structure of the biological cells. There were many pore structures between the particle and the nanoparticles uniformly distributed on the surface of the sample. **Figure 3B** shows the particle size of the sample was less than 20 nm, which was in accordance with the particle size calculated by JADE software. It can be seen from **Figure 3C** that the mean particle size of CeO_2 particles was about 9 nm. The selected area electron diffraction (SAED) pattern of micro-nano hierarchical ceria materials as showed in **Figure 3D**, confirmed the prepared sample was composed of ceria nanoparticles with high crystallinity and polycrystalline structure. On the surface of micro-nano hierarchical ceria materials, there were many irregular cellular structure polycrystalline particles, whose size was about 100 nm and existed plenty of pore structure. These results confirm that the micro-nano hierarchical ceria materials with the fiber structure were formed by self-assembly.

X-ray Diffraction Analysis

Figure 4 shows the XRD pattern of micro-nano hierarchical ceria materials. The six characteristic peaks of micro-nano hierarchical ceria materials sequentially correspond to (111), (200), (220), (311), (222), and (400) crystal planes of the face-centered cubic CeO_2 with standard JCPDF card No. 34-0394, indicating that the prepared product is a cerium oxide material. No extra peaks were observed, indicating that the template had been completely removed during the calcination and that the cerium nitrate precursor was thoroughly decomposed and the phase purity of the product was improved. The sharp diffraction peak and high XRD intensity of the sample indicated that the product has good crystallinity. According to the full width at half maximum (FWHM) of each diffraction peak, the grain size of micro-nano hierarchical cerium oxide material is calculated by the Scherrer formula to be 9 nm. The theoretical calculation result is consistent with the TEM observation.

Adsorption-Desorption Isotherm and Pore Size Distribution

Figure 5 shows the nitrogen adsorption-desorption isotherms and their corresponding pore size distribution curves of micro-nano hierarchical ceria materials. It can be observed that the adsorption-desorption isotherm is type IV and is a typical adsorption isotherm for both microporous and mesoporous structures. When the relative pressure increases to a certain

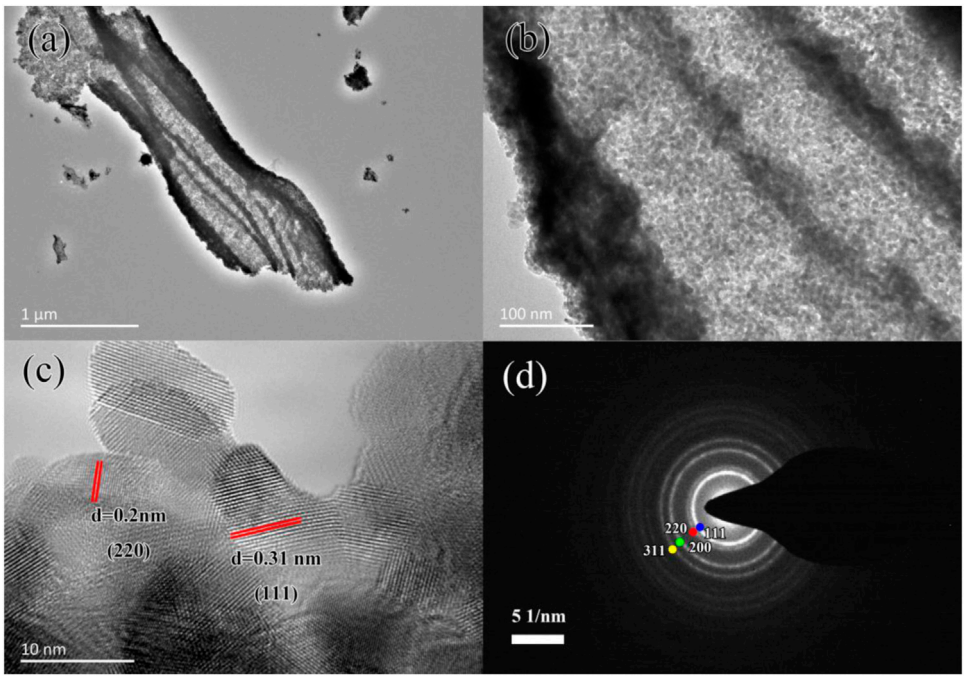

FIGURE 3 | (A) TEM image, **(B)** TEM enlargement, **(C)** HRTEM image, and **(D)** SAED pattern of micro-nano hierarchical ceria materials.

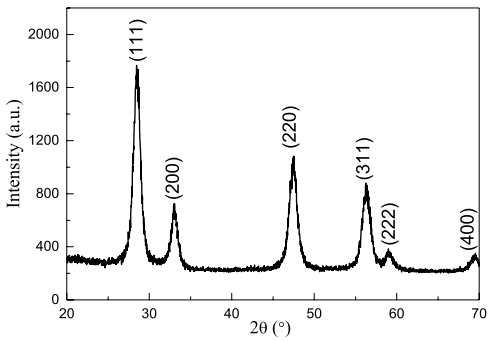

FIGURE 4 | XRD pattern of micro-nano hierarchical ceria materials.

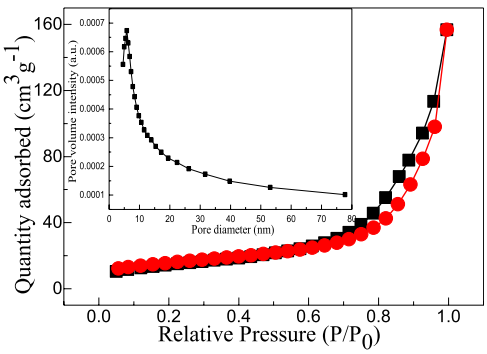

FIGURE 5 | Nitrogen adsorption-desorption isotherm of micro-nano hierarchical ceria materials. The inset shows the corresponding pore size distribution curve of micro-nano hierarchical ceria materials.

value (p/p_0 is 0.4–10), the nitrogen molecules in mesopores Capillary condensation occur, resulting in adsorption lag phenomenon, and the formation of an H3-type hysteresis ring. The position of the pressure section determines the pore size of micro-nano hierarchical ceria materials. The specific surface area of micro-nano hierarchical ceria materials calculated by the BET method was 55.6 m^2/g. The pore size distribution curve of micro-nano hierarchical ceria materials calculated by the BJH equation shows that the prepared fibrous cerium oxide material has more pore size distribution intervals and the diameters are between 4 and 20 nm, which fully shows that the sample was a rich mesoporous structure, which is consistent with the TEM observation. The existence of these mesoporous structures can increase the BET specific surface area of micro-nano hierarchical ceria materials, and then provide more active sites for the photocatalyst, and further enhance the photocatalytic activity of micro-nano hierarchical ceria materials.

Temperature-Programmed Reduction Experiments

H_2-TPR is the spectrum obtained according to the change of hydrogen concentration in the constant rate heating process, in which hydrogen in the reaction gas reacts with oxygen released in the transformation process of Ce^{4+}/Ce^{3+} to generate water. According to the peak temperature, peak type and peak area of the TPR spectrum, the catalytic, oxygen storage and release properties of micro-nano hierarchical ceria materials and bulk

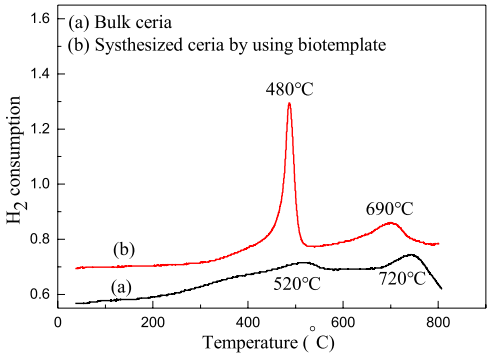

FIGURE 6 | Temperature-programmed reduction profiles of (a) micro-nano hierarchical ceria materials and (b) bulk ceria.

ceria can be qualitatively analyzed. **Figure 6** shows the temperature-programmed reduction profiles of micro-nano hierarchical ceria materials and bulk ceria. In **Figure 6**, bulk cerium oxide exhibits hydrogen consumption peaks at about 450 and 750°C, respectively, corresponding to surface and bulk oxygen consumption of cerium oxide materials. It can be clearly observed that the micro-nano hierarchical ceria materials prepared by the template method have a sharp peak type at about 480°C, and the peak area is much higher than that of bulk ceria. Simultaneously, the bulk phase oxygen consumption peak area of micro-nano hierarchical ceria materials is significantly reduced compared with the bulk ceria, indicating that the surface oxygen consumption of porous cerium oxide material is significantly increased. The results indicate that the micro-nano hierarchical ceria materials have more surface oxygen and more surface oxygen active sites. However, the hydrogen consumption peak of bulk phase oxygen appears at about 680°C, which may be caused by the crystal lattice distortion caused by the incorporation of N element in the template, which makes bulk phase oxygen overflow more easily. The above analysis results imply that the micro-nano hierarchical ceria materials have excellent photocatalytic activity.

Optical Properties

Figures 7A, B shows the UV–Vis absorption spectra of micro-nano hierarchical ceria materials and bulk ceria. As can be seen from **Figure 7A**, bulk CeO_2 has a high optical absorption coefficient before 400 nm and can respond to ultraviolet light. The micro-nano hierarchical ceria materials exhibit novel optical properties compared with those of bulk materials, and a new characteristic peak appears at about 380 nm, mainly due to special defects in the micro-nano hierarchical ceria materials. Meanwhile, the range of light absorption is extended from the ultraviolet region to the visible region. There is some weak light absorption at 600 and 700 nm, indicating that the micro-nano hierarchical ceria materials have a visible light response-ability. Based on UV-Vis absorption spectra and Tauc theory (Tang et al., 2020; Zhao et al., 2020; Gao et al., 2021a; Wang et al., 2021e), the optical band gap (Eg) value of bulk ceria and micro-nano hierarchical ceria materials can be obtained.

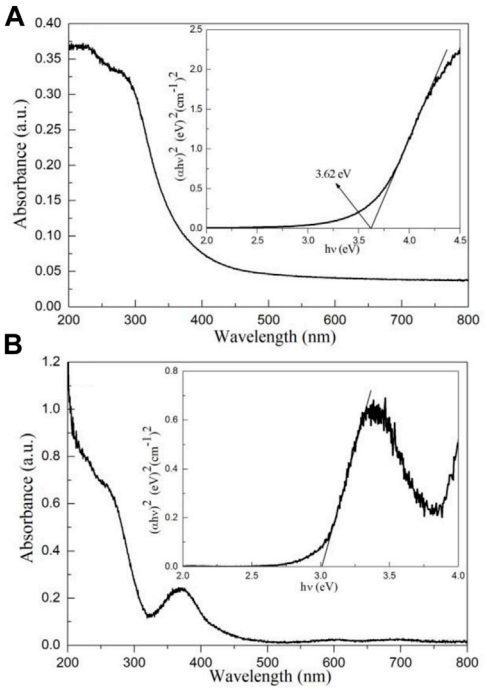

FIGURE 7 | UV–Vis absorption spectra of **(A)** bulk ceria and **(B)** micro-nano hierarchical ceria materials. The insets show the optical band gap (Eg) values of **(A)** bulk ceria and **(B)** micro-nano hierarchical ceria materials.

$$(F(R)h\nu)^n = A\left(h\nu - E_g\right) \quad (2)$$

Where ν is the frequency, A is the absorption coefficient, and $n = 2$.

The Eg values of bulk ceria and micro-nano hierarchical ceria materials as shown in **Figure 7A** inset and **Figure 7B** inset. The Eg values of bulk ceria and micro-nano hierarchical ceria materials are found to be 3.62 and 3.00 eV, respectively. The results show that the micro-nano hierarchical ceria materials can respond to visible light and is a potential visible-light photocatalyst. This conclusion will be further confirmed in the photocatalytic experiment section.

Photocatalytic Activity

To study the photocatalytic activity of micro-nano hierarchical ceria materials, methylene blue was selected as the target degradation dye (**Figure 8A**). To eliminate the influence of adsorption on the photocatalytic experiment, half an hour of adsorption experiments was carried out in a dark room before the photocatalytic experiment. Although CeO_2 forms a porous structure, the amount of methylene blue dye adsorbed is very low, only about 8%. When only the methylene blue dye solution is illuminated, the methylene blue dye hardly degrades. The results show that methylene blue dye is an organic pollutant that is difficult to degrade under natural light irradiation. To compare with the traditional CeO_2 nanoparticles (C-CeO_2), the photo-degradation of methylene blue dye by CeO_2 nanoparticles was also performed. The photocatalytic degradation rate increases

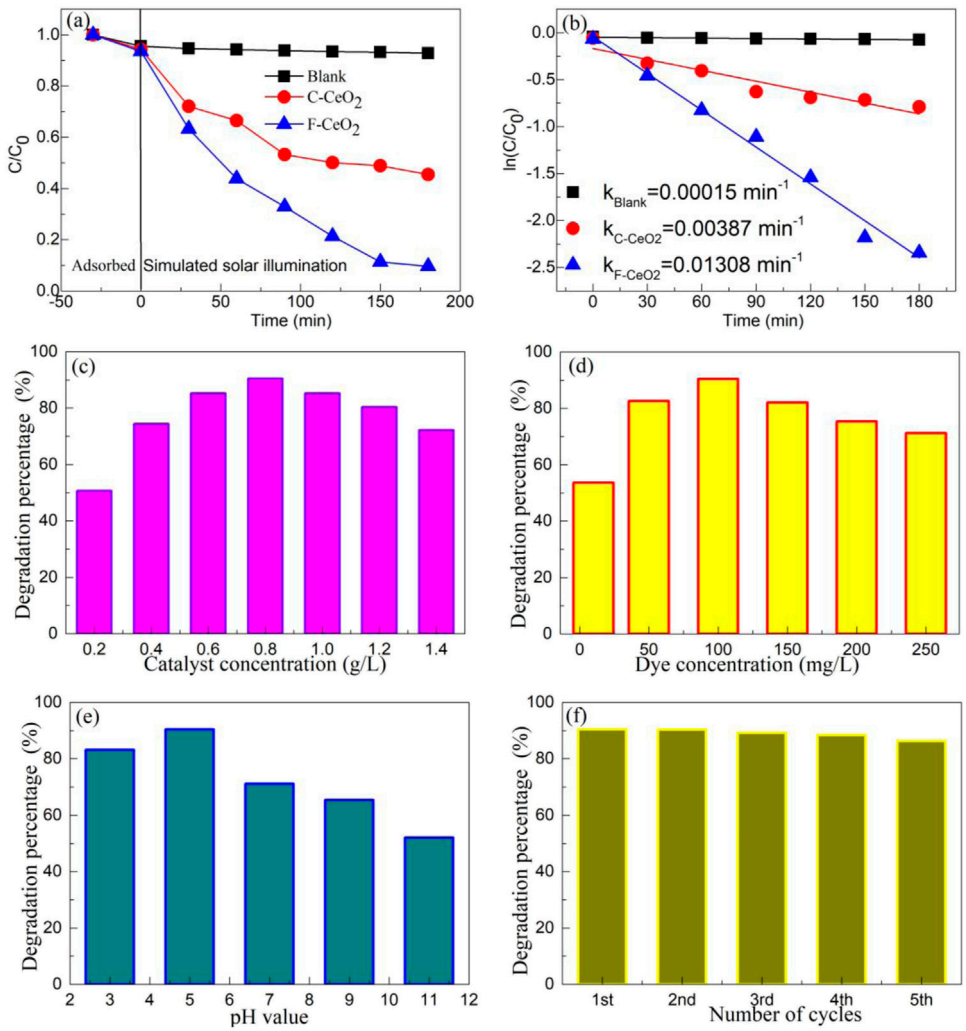

FIGURE 8 | Photocatalytic activity of micro-nano hierarchical ceria materials for the degradation of methylene blue under different parameters. **(A)** Different irradiation times, **(B)** Corresponding first-order dynamics curve, **(C)** Different catalyst concentrations, **(D)** Different dye concentrations, **(E)** Different pH values, and **(F)** Cyclic stability experiments.

with the increase of irradiation time. However, the degradation percentage of traditional CeO_2 nanoparticles was only about 50% after being exposed to light for 180 min. The photocatalytic degradation percentage of micro-nano hierarchical ceria materials can reach about 90.4%.

The degradation rate of micro-nano hierarchical ceria materials can be further expressed by first-order kinetic model (Wang et al., 2020b; Yu and Han, 2021):

$$\ln(A_t/A_0) = -kt \quad (3)$$

Where A_t, A_0, k, and t are the absorbance of dye at different irradiation times, the initial dye absorbance, the rate constant, and the irradiation time, respectively. The corresponding first-order dynamics curve of blank, the CeO_2 nanoparticles, and micro-nano hierarchical ceria materials is shown in **Figure 8B**. The k values of blank, CeO_2 nanoparticles, and micro-nano hierarchical ceria materials are 0.00015, 0.00387, and 0.01308 min^{-1}, respectively. The photocatalytic activity of micro-nano hierarchical ceria materials was about 3.38 times higher than that of CeO_2 nanoparticles. The photocatalytic activity of micro-nano hierarchical ceria materials was 2.60 times higher than that of CeO_2 nanoparticles reported in the literature (Gao et al., 2018a). The results further confirmed that the micro-nano hierarchical ceria materials exhibited high visible-light photocatalytic activity for the photo-degradation of methylene blue dye.

The effect of catalyst concentration on the photocatalytic activity of semiconductor photocatalysts is always a problem worth discussing. **Figure 8C** shows the effect of catalyst concentration on the photocatalytic activity of micro-nano hierarchical ceria materials for the photo-degradation of methylene blue under simulated solar irradiation. With the increase of catalyst concentration, the photocatalytic degradation percentage first increases and then decreases, and

the optimal catalyst concentration is 0.8 g/L. When the catalyst concentration is low, the probability of photon absorption is small, the photogenerated electron-hole pair is less, the number of catalytic active centers is correspondingly less, and the organic molecules can not be fully adsorbed to the surface of the micro-nano hierarchical ceria materials, so the photocatalytic degradation effect is poor. (Cao et al., 2018). With the increase of catalyst concentration, the utilization rate of photons increases, the number of catalytic active centers in the reaction increases, and the degradation rate increases. When the concentration of catalyst increases to a certain value (0.8 g/L), the photocatalytic degradation percentage reaches the best. When the concentration of catalyst continues to increase, the scattering effect of catalyst particles on incident light becomes prominent, and the utilization rate of photons decreases, making the degradation rate show a downward trend. (Yumei Guo et al., 2020).

Figure 8D shows the effect of dye concentration on the photocatalytic activity of micro-nano hierarchical ceria materials for the photo-degradation of methylene blue dye under simulated solar irradiation. With the increase of the methylene blue dye initial concentration, the degradation percentage first increased and then showed a downward trend, and the degradation percentage reached the maximum when the dye concentration was 100 mg/L. When the dye concentration is low, the photocatalytic reaction rate is approximately proportional to the concentration of organic matter (Konstantinou and Albanis, 2004), so the degradation percentage of dye increases with the increase of dye concentration. When the dye concentration is too high, the transmittance of the solution decreases, resulting in a decrease in the number of effective photons involved in the photocatalytic reaction, and the surface of the catalyst will reduce its active site due to the adsorption of excessive dye molecules. (Wang and Tian, 2020). When the concentration of dye molecules exceeds a certain level, its degradation rate begins to decline.

Figure 8E shows the effect of pH value on the photocatalytic activity of micro-nano hierarchical ceria materials for the photo-degradation of methylene blue dye under simulated solar irradiation. It can be seen from **Figure 8E** that the degradation percentage of methylene blue dye is higher in acidic conditions, but lower in alkaline conditions. The optimal pH value of micro-nano hierarchical ceria materials for the photo-degradation of methylene blue dye under simulated solar irradiation is 5. This result is related to the point of zero charge (PZC) of CeO_2 and the cationic dye of methylene blue. (Gao et al., 2018b; Ramirez et al., 2019).

The recyclability of a photocatalyst is another important index to evaluate its photocatalytic activity. **Figure 8F** shows the recyclability experiments of micro-nano hierarchical ceria materials for the photo-degradation of methylene blue dye under simulated solar irradiation. After each cycle, the photocatalyst in the degraded dye solution should be centrifuged, filtered, and dried before the next cycle experiment. After five cycles, the degradation rate of micro-nano hierarchical ceria materials decreased by only about 6%, indicating that the micro-nano hierarchical ceria materials can be reused many times. The results indicate that the micro-nano hierarchical ceria materials have high cyclic stability and are a potential visible-light photocatalyst.

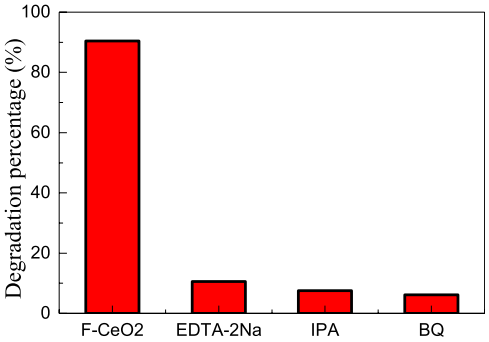

FIGURE 9 | Species trapping experiments for the degradation of methylene blue dye over micro-nano hierarchical ceria materials.

Photocatalytic Mechanism

Based on the literature (He et al., 2016; He et al., 2021), the hole (hVB+), hydroxyl radical (•OH) and superoxide radical ($\bullet O_2^-$) can be detected by using the disodium ethylenediamine tetraacetic acid (EDTA-2Na), 2-propanol (IPA), and 1, 4-benzoquinone (BQ) as scavengers, respectively. The trapping experiment was consistent with the photocatalytic experiment, except that a 1 mmol trapping agent was added to the reaction solution. **Figure 9** shows the species trapping experiments for the degradation of methylene blue dye over micro-nano hierarchical ceria materials. When EDTA-2Na, IPA, and BQ were added to the reaction solution, the photocatalytic efficiency of micro-nano hierarchical ceria materials was significantly inhibited, indicating that holes, hydroxyl radicals, and superoxide radicals played a crucial role in the photocatalytic reaction.

Based on the experimental results and band theory analysis, the photocatalytic mechanism of micro-nano hierarchical ceria materials can be discussed. The adsorption experiment results show that the effect of adsorption on micro-nano hierarchical ceria materials is very small. According to the literature (Gao et al., 2018a) and the Eg value of micro-nano hierarchical ceria materials, the conduction band potential and valence band potential of micro-nano hierarchical ceria materials were obtained. **Figure 10** shows the photocatalytic mechanism of micro-nano hierarchical ceria materials. When simulated sunlight shines on the surface of micro-nano hierarchical ceria materials, photogenerated electrons are excited to transition to the conduction band of micro-nano hierarchical ceria materials, leaving holes in the valence band.

$$\text{Ceria} + \text{hv} \rightarrow \text{e}^- + \text{h}^+ \quad (4)$$

Some of the remaining holes in the valence band react directly with the dye to form non-toxic small molecular organic matters, while the other reacts with OH^- or H_2O to form hydroxyl radicals (•OH).

$$h^+ + \text{dye} \rightarrow \text{Products} \quad (5)$$

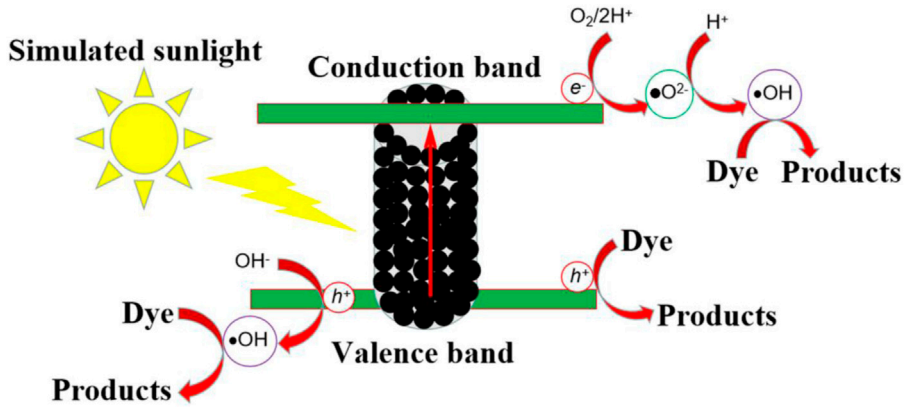

FIGURE 10 | Photocatalytic mechanism of micro-nano hierarchical ceria materials.

$$h^+ + OH^-/H_2O \rightarrow \bullet OH \quad (6)$$

The electrons that transition to the conduction band will undergo a series of reactions, forming superoxide radicals ($\bullet O^{2-}$), which in turn interact with the electrons to form •OH (Li et al., 2019; You et al., 2020; Zheng et al., 2020; Dhinagaran et al., 2021).

$$e^- + O_2 \rightarrow \bullet O^{2-} \quad (7)$$

$$\bullet O^{2-} + 2H^+ + e^- \rightarrow H_2O_2 \quad (8)$$

$$2e^- + O_2 + 2H^+ \rightarrow H_2O_2 \quad (9)$$

$$e^- + H_2O_2 \rightarrow \bullet OH + OH^- \quad (10)$$

$$\bullet O^{2-} + H_2O_2 \rightarrow \bullet OH + OH^- + O_2 \quad (11)$$

Hydroxyl radicals generated in the conduction band or valence band of micro-nano hierarchical ceria materials will interact with dye molecules to produce non-toxic and harmless products.

$$\bullet OH + \text{dye} \rightarrow \text{Products} \quad (12)$$

When the dye and micro-nano hierarchical ceria materials adsorb together by electrostatic interaction (Ayati et al., 2016; Gao et al., 2021b; Liu et al., 2022), in addition to the interaction of holes, superoxide radical, and hydroxyl radical, the special defect structure of micro-nano hierarchical ceria materials also causes the degradation of the dye. Combined with experimental analysis results and mechanism study, the special defects in the micro-nano hierarchical ceria materials also play an important role in the photo-degradation of methylene blue dye. Analysis of the results shows that the defect plays the role of electron transport carrier in the transfer and separation of charge carriers.

CONCLUSION

The micro-nano hierarchical ceria materials were prepared using the oriental paperbush flower stems as a template and cerium nitrate as a precursor. The fiber length ranged from 100 to 500 μm and the radius was about 3–8 μm. The fiber structure was warped due to inconsistent shrinkage in the subsequent calcination process and formed a hollow-like structure. The micro-nano hierarchical ceria materials have a large BET-specific surface area (55.6 m^2/g) and abundant pore structures, which can increase the BET-specific surface area and promote the mass transfer process. HRTEM imaging shows that the fiber structure is composed of uniformly distributed nano-polycrystalline cerium oxide grains. There are many active oxygen sites on the surface of micro-nano hierarchical ceria materials, but the doping of N element in the template causes the lattice distortion of cerium oxide. The micro-nano hierarchical ceria materials showed the best photocatalytic activity for the photodegradation of methylene blue under visible light irradiation, and the degradation percentage of methylene blue reached 90.4% after 180 min. The optimal irradiation time, catalyst concentration, dye concentration, and pH value were 180 min, 0.8 g/L, 100 mg/L, and 5, respectively. This method can be used to synthesize other micro-nano hierarchical metal oxides and enhance their physicochemical properties.

DATA AVAILABILITY STATEMENT

The original contributions presented in the study are included in the article/supplementary material, further inquiries can be directed to the corresponding authors.

AUTHOR CONTRIBUTIONS

MeZ was responsible for synthesis experiments, performance tests and data analysis. XC, MiZ and YT were responsible for material characterization. CL was responsible for the analysis and guidance of XRD and UV tests. WL is responsible for analyzing the reaction mechanism. FC was responsible for experimental design and paper revision.

FUNDING

This work was supported by the National key research and development plan of "air pollution causes and control technology research" (2017YFC0211903), National Natural Science Foundation of China (21773291), the Natural Science Foundation of Jiangsu Province (BK20180103), the Qing Lan Project of Jiangsu Province and Postgraduate research and innovation plan project in Jiangsu Province (KYCX20_2761).

REFERENCES

Ai, K., Huang, J., Xiao, Z., Yang, Y., Bai, Y., and Peng, J. (2021). Localized Surface Plasmon Resonance Properties and Biomedical Applications of Copper Selenide Nanomaterials. *Mater. Today Chem.* 20, 100402. doi:10.1016/j.mtchem.2020.100402

Ayati, A., Shahrak, M. N., Tanhaei, B., and Sillanpää, M. (2016). Emerging Adsorptive Removal of Azo Dye by Metal-Organic Frameworks. *Chemosphere* 160, 30–44. doi:10.1016/j.chemosphere.2016.06.065

Caballero-Espitia, D. L., Lizarraga-Medina, E. G., Borbon-Nuñez, H. A., Contreras-Lopez, O. E., Tiznado, H., and Marquez, H. (2020). Study of Al2O3 Thin Films by ALD Using H2O and O3 as Oxygen Source for Waveguide Applications. *Opt. Mater.* 109, 110370. doi:10.1016/j.optmat.2020.110370

Cao, Z., Wang, C., and Chen, J. (2018). Synthesis and Photocatalytic Property of P-N junction YMnO3/SrTiO3 Composites. *Mater. Res. Express* 5, 115512. doi:10.1088/2053-1591/aadec0/meta#

Chen, S., Skordos, A., and Thakur, V. K. (2020). Functional Nanocomposites for Energy Storage: Chemistry and New Horizons. *Mater. Today Chem.* 17, 100304. doi:10.1016/j.mtchem.2020.100304

Chenab, K. K., Sohrabi, B., Jafari, A., and Ramakrishna, S. (2020). Water Treatment: Functional Nanomaterials and Applications from Adsorption to Photodegradation. *Mater. Today Chem.* 16, 100262. doi:10.1016/j.mtchem.2020.100262

Cheng, T., Gao, H., Li, R., Wang, S., Yi, Z., and Yang, H. (2021). Flexoelectricity-induced Enhancement in Carrier Separation and Photocatalytic Activity of a Photocatalyst. *Appl. Surf. Sci.* 566, 150669. doi:10.1016/j.apsusc.2021.150669

Cheng, T., Gao, H., Sun, X., Xian, T., Wang, S., Yi, Z., et al. (2021). An Excellent Z-Scheme Ag2MoO4/Bi4Ti3O12 Heterojunction Photocatalyst: Construction Strategy and Application in Environmental Purification. *Adv. Powder Tech.* 32 (3), 951–962. doi:10.1016/j.apt.2021.01.039

Dhinagaran, M., Elakkiya, V., and Sumathi, S. (2021). Tailor Made ZnAl2O4-CeO2 Hetero Structure as an Efficient Photo Catalyst for Environmental Remediation. *Opt. Mater.* 111, 110546. doi:10.1016/j.optmat.2020.110546

Gao, H. J., Wang, S. F., Fang, L. M., Sun, G. A., Chen, X. P., Tang, S. N., et al. (2021). Nanostructured Spinel-type M(M = Mg, Co, Zn)Cr2O4 Oxides: Novel Adsorbents for Aqueous Congo Red Removal. *Mater. Today Chem.* 22, 100593. doi:10.1016/j.mtchem.2021.100593

Gao, H., Wang, Y., Gao, Q., Pan, X., Wang, S., Yang, H., et al. (2021). Phase Evolution and Photoluminescence Behavior of MMoO4 (M = Mg, Ca, Sr) Phosphors. *Optik* 241, 167040. doi:10.1016/j.ijleo.2021.167040

Gao, H., Yang, H., and Wang, S. (2018). Hydrothermal Synthesis, Growth Mechanism, Optical Properties and Photocatalytic Activity of Cubic SrTiO3 Particles for the Degradation of Cationic and Anionic Dyes. *Optik* 175, 237–249. doi:10.1016/j.ijleo.2018.09.027

Gao, H., Yang, H., Yang, G., and Wang, S. (2018). Effects of Oxygen Vacancy and Sintering Temperature on the Photoluminescence Properties and Photocatalytic Activity of CeO2 Nanoparticles with High Uniformity. *Mater. Tech.* 33, 321–332. doi:10.1080/10667857.2018.1438222

Ge, Y., Luo, H., Huang, J., and Zhang, Z. (2021). Visible-light-active TiO2 Photocatalyst for Efficient Photodegradation of Organic Dyes. *Opt. Mater.* 115, 111058. doi:10.1016/j.optmat.2021.111058

Gong, X., Gao, X., Du, W., Zhang, H., Zhang, S., Nguyen, T. T., et al. (2019). Wood Powder-Derived Quantum Dots for CeO2 Photocatalytic and Anti-counterfeit Applications. *Opt. Mater.* 96, 109302. doi:10.1016/j.optmat.2019.109302

Han, K., Wang, Y., Wang, S., Liu, Q., Deng, Z., and Wang, F. (2021). Narrowing Band gap Energy of CeO2 in (Ni/CeO2)@SiO2 Catalyst for Photothermal Methane Dry Reforming. *Chem. Eng. J.* 421, 129989. doi:10.1016/j.cej.2021.129989

He, Z., Xia, Y., Tang, B., Jiang, X., and Su, J. (2016). Fabrication and Photocatalytic Property of ZnO/Cu2O Core-Shell Nanocomposites. *Mater. Lett.* 184, 148–151. doi:10.1016/j.matlet.2016.08.020

He, Z., Yang, H., Su, J., Xia, Y., Fu, X., Kang, L., et al. (2021). Polyacrylamide Gel Synthesis and Photocatalytic Performance of CuCo2O4 Nanoparticles. *Mater. Lett.* 288, 129375. doi:10.1016/j.matlet.2021.129375

Jiménez-Almarza, A., López-Magano, A., Cano, R., Ortín-Rubio, B., Díaz-García, D., Gomez-Ruiz, S., et al. (2021). Engineering Covalent Organic Frameworks in the Modulation of Photocatalytic Degradation of Pollutants under Visible Light Conditions. *Mater. Today Chem.* 22, 100548. doi:10.1016/j.mtchem.2021.100548

Konstantinou, I. K., and Albanis, T. A. (2004). TiO2-assisted Photocatalytic Degradation of Azo Dyes in Aqueous Solution: Kinetic and Mechanistic Investigations. *Appl. Catal. B: Environ.* 49, 1–14. doi:10.1016/j.apcatb.2003.11.010

Kulshrestha, A., Gehlot, P. S., and Kumar, A. (2021). Paramagnetic Surface Active Ionic Liquids: Synthesis, Properties, and Applications. *Mater. Today ChemistryToday Chem* 21, 100522. doi:10.1016/j.mtchem.2021.100522

Li, D., Zu, X., Ao, D., Tang, Q., Fu, Y., Guo, Y., et al. (2019). High Humidity Enhanced Surface Acoustic Wave (SAW) H2S Sensors Based on Sol-Gel CuO Films. *Sensors Actuators B: Chem.* 294, 55–61. doi:10.1016/j.snb.2019.04.010

Li, J., Wang, S., Sun, G., Gao, H., Yu, X., Tang, S., et al. (2021). Facile Preparation of MgAl2O4/CeO2/Mn3O4 Heterojunction Photocatalyst and Enhanced Photocatalytic Activity. *Mater. Today Chem.* 19, 100390. doi:10.1016/j.mtchem.2020.100390

Liu, H., Wang, S., Gao, H., Yang, H., Wang, F., Chen, X., et al. (2022). A Simple Polyacrylamide Gel Route for the Synthesis of MgAl2O4 Nanoparticles with Different Metal Sources as an Efficient Adsorbent: Neural Network Algorithm Simulation, Equilibrium, Kinetics and Thermodynamic Studies. *Sep. Purif. Tech.* 281, 119855. doi:10.1016/j.seppur.2021.119855

Medda, S. K., Manna, S., and De, G. (2020). Photocatalytic Evaluation of Anatase TiO2 Coating on Ceramic Tiles by Raman Spectroscopy. *Trans. Indian Ceram. Soc.* 79, 13–17. doi:10.1080/0371750X.2019.1696233

Murali, A., Lan, Y. P., Sarswat, P. K., and Free, M. L. (2019). Synthesis of CeO2/reduced Graphene Oxide Nanocomposite for Electrochemical Determination of Ascorbic Acid and Dopamine and for Photocatalytic Applications. *Mater. Today Chem.* 12, 222–232. doi:10.1016/j.mtchem.2019.02.001

Pooja, P., and Chowdhury, P. (2021). Functionalized CdTe Fluorescence Nanosensor for the Sensitive Detection of Water Borne Environmentally Hazardous Metal Ions. *Opt. Mater.* 111, 110584. doi:10.1016/j.optmat.2020.110584

Ramirez, L., Ramseier Gentile, S., Zimmermann, S., and Stoll, S. (2019). Behavior of TiO2 and CeO2 Nanoparticles and Polystyrene Nanoplastics in Bottled Mineral, Drinking and Lake Geneva Waters. Impact of Water Hardness and Natural Organic Matter on Nanoparticle Surface Properties and Aggregation. *Water* 11 (4), 721. doi:10.3390/w11040721

Tang, S., Wang, S., Yu, X., Gao, H., Niu, X., Wang, Y., et al. (2020). Gamma-Ray Irradiation Assisted Polyacrylamide Gel Synthesis of Scheelite Type BaWO 4 Phosphors and its Colorimetric, Optical and Photoluminescence Properties. *ChemistrySelect* 5, 10599–10606. doi:10.1002/slct.202002429

Wang, S.-F., Zhang, C., Sun, G., Chen, B., Xiang, X., Wang, H., et al. (2013). Fabrication of a Novel Light Emission Material AlFeO3 by a Modified Polyacrylamide Gel Route and Characterization of the Material. *Opt. Mater.* 36, 482–488. doi:10.1016/j.optmat.2013.10.014

Wang, S. F., Chen, X. Y., Gao, H. J., Fang, L. M., Hu, Q. W., Sun, G. A., et al. (2021). A Comparative Study on the Phase Structure, Optical and NIR Reflectivity of BaFe12O19 Nano-Pigments by the Traditional and Modified Polyacrylamide Gel Method. *JNanoR* 67, 1–14. doi:10.4028/www.scientific.net/jnanor.67.1

Wang, S., Gao, H., Fang, L., Hu, Q., Sun, G., Chen, X., et al. (2021). Synthesis of Novel CQDs/CeO2/SrFe12O19 Magnetic Separation Photocatalysts and

Synergic Adsorption-Photocatalytic Degradation Effect for Methylene Blue Dye Removal. *Chem. Eng. J. Adv.* 6, 100089. doi:10.1016/j.ceja.2021.100089

Wang, S., Gao, H., Li, J., Wang, Y., Chen, C., Yu, X., et al. (2021). Comparative Study of the Photoluminescence Performance and Photocatalytic Activity of CeO2/MgAl2O4 Composite Materials with an N-N Heterojunction Prepared by One-step Synthesis and Two-step Synthesis Methods. *J. Phys. Chem. Sol.* 150, 109891. doi:10.1016/j.jpcs.2020.109891

Wang, S., Gao, H., Yu, H., Li, P., Li, Y., Chen, C., et al. (2020). Optical and Photoluminescence Properties of the MgAl2O4:M (M = Ti, Mn, Co, Ni) Phosphors: Calcination Behavior and Photoluminescence Mechanism. *Trans. Indian Ceram. Soc.* 79, 221–231. doi:10.1080/0371750X.2020.1817789

Wang, S., Gao, H., Yu, X., Tang, S., Wang, Y., Fang, L., et al. (2020). Nanostructured SrTiO3 with Different Morphologies Achieved by mineral Acid-Assisted Hydrothermal Method with Enhanced Optical, Electrochemical, and Photocatalytic Performances. *J. Mater. Sci. Mater. Electron.* 31, 17736–17754. doi:10.1007/s10854-020-04328-0

Wang, S., Tang, S., Gao, H., Chen, X., Liu, H., Yu, C., et al. (2021). Microstructure, Optical, Photoluminescence Properties and the Intrinsic Mechanism of Photoluminescence and Photocatalysis for the BaTiO3, BaTiO3/TiO2 and BaTiO3/TiO2/CeO2 Smart Composites. *Opt. Mater.* 118, 111273. doi:10.1016/j.optmat.2021.111273

Wang, S., Tang, S., Gao, H., Fang, L., Hu, Q., Sun, G., et al. (2021). Modified Polyacrylamide Gel Synthesis of CeO2 Nanoparticles by Using Cerium Sulfate as Metal Source and its Optical and Photoluminescence Properties. *J. Mater. Sci. Mater. Electron.* 32, 10820–10834. doi:10.1007/s10854-021-05740-w

Wang, Y., and Tian, H. (2020). Study on the Construction of YMnO3/CeO2 Composite Photocatalyst Heterostructure and Photocatalytic Degradation of Methyl Red. *Optik* 201, 163524. doi:10.1016/j.ijleo.2019.163524

Wu, S., Liu, Y., He, L., and Wang, F. (2004). Preparation of β-spodumene-based Glass-Ceramic Powders by Polyacrylamide Gel Process. *Mater. Lett.* 58, 2772–2775. doi:10.1016/j.matlet.2004.04.017

Xian, T., Yang, H., Shen, X., Jiang, J. L., Wei, Z. Q., and Feng, W. J. (2009). Preparation of High-Quality BiFeO3 Nanopowders via a Polyacrylamide Gel Route. *J. Alloys Comp.* 480, 889–892. doi:10.1016/j.jallcom.2009.02.068

You, J., Zhan, S., Wen, J., Ma, Y., and Zhu, Z. (2020). Construction of Heterojunction of Ag2S Modified Yttrium Manganate Visible Photocatalyst and Study on Photocatalytic Mechanism. *Optik* 217, 164900. doi:10.1016/j.ijleo.2020.164900

Yu, H., and Han, Q. (2021). Effect of Reaction Mediums on Photocatalytic Performance of BiOX (X = Cl, Br, I). *Opt. Mater.* 119, 111399. doi:10.1016/j.optmat.2021.111399

Yumei Guo, Y., Ren, C., Li, L., and Zhang, X. (2020). Comparative Study of Cobalt Ferrite and Polyacrylamide Decorated Cobalt Ferrite Microspheres in Structural, Optical, Magnetic, Photoluminescence, and Photocatalytic Properties. *Russ. J. Phys. Chem.* 94, 2614–2621. doi:10.1134/S003602442012033X

Zhang, Y., Liang, H., Zhao, C. Y., and Liu, Y. (2009). Macroporous Alumina Monoliths Prepared by Filling Polymer Foams with Alumina Hydrosols. *J. Mater. Sci.* 44, 931–938. doi:10.1007/s10853-008-3189-6

Zhang, Y., Zhao, C. Y., Liang, H., and Liu, Y. (2009). Macroporous Monolithic Pt/γ-Al2O3 and K-Pt/γ-Al2O3 Catalysts Used for Preferential Oxidation of CO. *Catal. Lett.* 127, 339–347. doi:10.1007/s10562-008-9686-z

Zhao, X., Wang, S., Guan, S., Gao, H., Wang, Y., Wang, Y., et al. (2020). Construction and Photoluminescence Mechanism of N-N Type Double Heterojunction Bi2S3/Bi4Ti3O12/Bi2MoO6 Phosphors. *Optik* 224, 165537. doi:10.1016/j.ijleo.2020.165537

Zheng, Z., Zu, X., Zhang, Y., and Zhou, W. (2020). Rational Design of Type-II Nano-Heterojunctions for Nanoscale Optoelectronics. *Mater. Today Phys.* 15, 100262. doi:10.1016/j.mtphys.2020.100262

Conflict of Interest: The authors declare that the research was conducted in the absence of any commercial or financial relationships that could be construed as a potential conflict of interest.

Publisher's Note: All claims expressed in this article are solely those of the authors and do not necessarily represent those of their affiliated organizations, or those of the publisher, the editors, and the reviewers. Any product that may be evaluated in this article, or claim that may be made by its manufacturer, is not guaranteed or endorsed by the publisher.